Research Article

Hefei Zhou, Xiaoyang Zhu*, Hongke Li and Hongbo Lan*

Fabrication of the large-area flexible transparent heaters using electric-field-driven jet deposition micro-scale 3D printing

https://doi.org/10.1515/aot-2019-0021
Received February 14, 2019; accepted April 23, 2019; previously published online May 31, 2019

Abstract: In order to realize the mass production of the large-area flexible transparent film heater (FTFH) at low-cost, this paper presents a novel method which can achieve the direct fabrication of the large-area FTFH with Ag-grid by using an electric-field-driven jet deposition micro-scale 3D printing. The effects of the line width and the pitch of the printed Ag-grids on the optical transmittance and the sheet resistance are revealed. A typical FTFH with area of 80 mm × 60 mm, optical transmittance of 91.5% and sheet resistance of 4.7 Ω sq^{-1} is fabricated by the nano-silver paste with a high silver content (80 wt.%) and high viscosity (up to 20 000 mPa · s). Temperature-time response profiles and heating temperature distribution show that the heating performance of the FTFH has good thermal and mechanical properties. Furthermore, the adhesive force grade between the Ag-grid and the PET substrate measured to be 4B by 3M scotch tape. Therefore, the FTFH fabricated here is expected to be widely used in industry, such as window defroster of vehicles and display or touch screens owing to its striking characteristics of large area and low cost fabrication.

Keywords: Ag-grid; flexible transparent heater; micro-scale 3D printing.

***Corresponding authors: Xiaoyang Zhu,** Shandong Engineering Research Center for Additive Manufacturing, Qingdao University of Technology, Qingdao 266520, China, e-mail: zhuxiaoyang@qtech.edu.cn; and **Hongbo Lan,** Shandong Engineering Research Center for Additive Manufacturing, Qingdao University of Technology, Qingdao 266520, China; and Qingdao Engineering Research Center for 3D Printing, Qingdao University of Technology, Qingdao 266520, China, e-mail: hblan99@126.com
Hefei Zhou and Hongke Li: Shandong Engineering Research Center for Additive Manufacturing, Qingdao University of Technology, Qingdao 266520, China

© 2019 THOSS Media and De Gruyter

1 Introduction

Transparent film heaters (TFHs) have garnered significant attention for their wide applications such as, window defroster of vehicles, thermal therapies, display or touch screens, heating retaining windows and even soft actuators for soft robotics [1–5]. The TFHs conventionally comprise of transparent substrates and conductive materials or elements which cannot affect the transmittance of the substrate. The transmittance and sheet resistance of the TFHs are two important indexes and the trade-off between them is an added constraint. So far, the most common material applied is indium-doped tin oxides (ITO) for its relatively high electrical conductivity and optical transmittance as well as good environmental stability. However, the brittleness of ITO and the scarcity of the indium hinder the application for the flexible transparent film heaters (FTFH). In some applications e.g. wearable heaters and flexible displays, theyrequire not only good optical and electrical properties but also better stretchability and flexibility [6–8]. Recently, various emerging materials have been studied as the alternative materials of the ITO to overcome these ITO disadvantages, such as carbon nano-tube [9–12], graphene [13–15], conductive polymers [16, 17], metal nano-wires [8, 18–20], metal grids [21, 22] and hybrid films [23, 24]. While, the relatively higher sheet resistance of carbon nano-tube, graphene and conductive polymers [18], limit their applications [25], metal nano-wires and metal grids have emerged as two promising candidates to fabricate FTFH, which can theoretically exhibit superior electrical and optical properties compared to ITO.

Although both the metal nano-wires and metal grids exhibit good electrical and optical properties, there are still some limitations. For the mostly used Ag nano-wires, thermal stability at above 250°C is not good, the surface roughness of deposited nanowire networks is high and the adhesion between nanowire networks and substrates is poor [26]. These disadvantages limit the use of the Ag nano-wires at applications which require high

temperature and long term services. For the metal grids, the fabrication process is costly, especially for the fabrication of large-area metal grids, such as optical lithography [27] and nanoimprint lithography [28]. Inkjet printing [29] and aerosol printing [30] can achieve rapid printing of large area complex circuits and shorten the manufacturing process. However, they have a low printing resolution and a low printing capacity. Even though the aerosol jet printing resolution has been improved significantly, the viscosity of the printing materials is still below 1000 cps. However, the inks with high silver content generally have high viscosity, which is generally greater than 10 000 cps. Printing inks with high silver content can produce silver wires with high conductivity. In recent years, electrohydrodynamic (EHD) jet printing has shown great advantages in high viscosity and high resolution printing, but the EHD jet printing is prone to instability due to residual charge when printing conductive materials on insulating substrates. It is almost impossible to achieve stable printing and it is difficult to obtain large-area FTFH fabrication uniformly [31]. Consequently, there are still many challenges in the existing fabrication technologies to achieve mass production of high performance FTFH with low cost, especially the large area FTFH. For this reason, the present work herein is devoted to obtaining a method for low cost and high efficiency fabrication of the large area FTFH with high performance.

In this work, we demonstrate a large area FTFH with high performance based on a novel electric-field-driven (EFD) micro-scale 3D printing technology. A new electric field generation method in EFD micro-scale 3D printing effectively solves the problem of instability printing of conductive materials to insulating substrates in traditional EHD jet printing. A large area FTFH with a high performance was successfully fabricated based on the EFD micro-scale 3D printing. Due to the directness of the printing method, the transmittance and the sheet resistance can be easily controlled by changing the design of the Ag grid without using any photomask for conventional photolithography. Excellent electrothermal performances were obtained through the infrared thermal imaging and snow melting experiments. Furthermore, the fabricated FTFH also showed a stable electrothermal performance under continuous bending and twisting stress.

2 Experimental section

2.1 Fabrication method

Figure 1 depicts the manufacturing process of large area FTFH based on EFD micro-scale 3D printing. The line width and pitch of the metal grid can be determined and optimized by the technical specifications of heating power and optical transmittance required in practical applications. The EFD micro-scale 3D printer is independently developed and used to print the metal-grid on the flexible substrate cleaned by ultrasonic washer. The final FTFH with metal-grid can be obtained after the printed metal-grid is conductively treated by vacuum sintering, laser sintering or photon sintering.

Printing the metal-grid based on the EFD micro-scale 3D printing technology is the key process of the proposed method. EFD micro-scale 3D printing is a novel micro-scale 3D printing technology. Based on self-excited electric field, it utilizes EHD cone-jetting behavior and charge-induced self-alignment, and combines two novel working modes of pulsed cone jet and continuous cone-jet to achieve high-efficiency, low-cost and large-area micro-scale 3D printing. It has unique advantages and potential in multi-material multi-scale 3D printing and macro/micro cross-scale 3D printing. The forming principle of

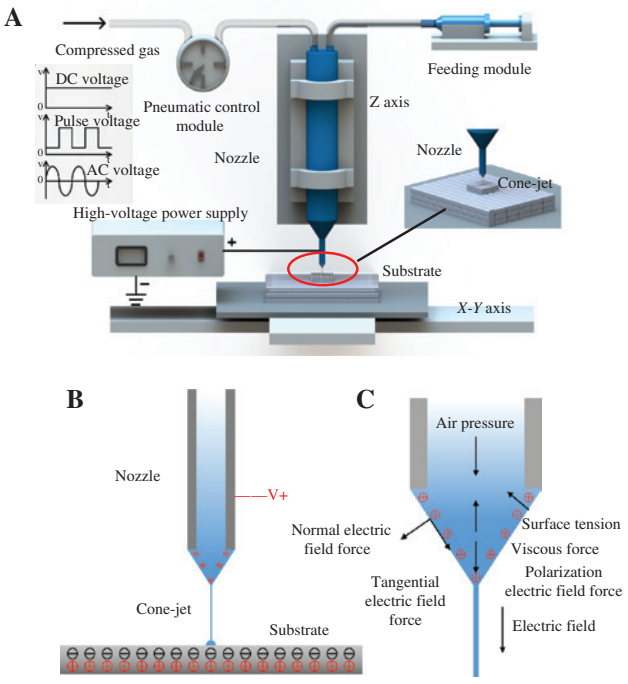

Figure 2: The forming principle of EFD micro-scale 3D printing. (A) Overall structure of the system; (B) induced electric field and charge distribution; (C) forces on microfluids and Taylor cones.

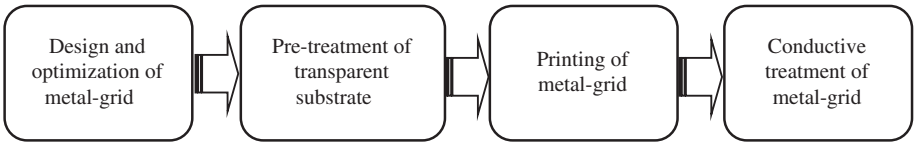

Figure 1: The manufacturing process of large area FTFH.

EFD micro-scale 3D printing is described in Figure 2. The EFD micro-scale 3D printing cannot only print micro-scale structures, but also print ultra-high viscosity materials (20 000 mPa · s). What's more, it improves the stability of printing when printing conductive materials on insulating substrates. At the same time, the EFD micro-scale 3D printing can achieve high resolution printing on non-conductive and non-uniform substrates. Therefore, an ideal solution for the efficient and low-cost fabrication of large area FTFH can be provided based on EFD micro-scale 3D printing the high metal content nano-paste.

2.2 Materials

The printing nozzle used in the experiment is a stainless steel needle with an inner diameter of 160 μm. The substrate is a transparent polyethylene terephthalate (PET) film with an area of 200 mm × 200 mm and 100 mm × 100 mm, and thickness of 0.2 mm. Considering the technological parameters such as viscosity, surface tension, silver content, adhesion force, sintering temperature and so on, the specific nano conductive silver paste developed independently with high viscosity and silver content is selected as the printing material. Table 1 shows the main physical performance parameters of the nano-silver.

2.3 Characterization

The optical transmittance of Ag-grids with different pitches and line widths was measured by ultraviolet/visible spectrophotometer (UV-6100, Shanghai Yuanyi Inc. China). The sheet resistance of Ag-grids with different pitches and line widths was measured by DC resistance tester (AT516, Changzhou Anbai Inc. China). The morphology of the Ag-grids were observed by field emission scanning electron microscopy (MERLIN Compact, ZEISS. Germany). The electrothermal performances of FTFH were measured by thermal imager (TG165, FLIR Systems. USA). The three-dimensional morphology and surface roughness data of the Ag-grids were measured by digital microscope (DSX510, OLYMPUS. Japan).

3 Results and discussion

3.1 Structural properties of large area FTFH

Based on the proposed method and self-made nano conductive silver paste, Ag-grids with different pitches and line widths were printed on the PET substrate and sintered in vacuum furnace at 60°C for 60 min to complete the conductive treatment of silver wire. Figure 3 shows the macroscopic and microscopic morphology of the FTFH with an area of 200 mm × 200 mm, line width of 25 μm, and pitch of 3 mm. As shown in the picture, the thickness of the Ag-grid is 3.26 μm, and the surface roughness of the Ag-grids is 0.763 μm(Ra). The printed Ag-grid has good consistency and surface morphology after being sintered. The silver wire is continuous, uniform and without breakpoints. Furthermore, silver particles are well-distributed, and there is no suspension and overlap phenomenon in the cross connection of the Ag-grid. Meanwhile, the adhesive force between the Ag-grid and the PET substrate was measured as 4B using 3M scotch tape. Preliminary conclusion can be drawn from the figure that EFD micro-scale 3D printing is capable of printing a large area of Ag-grid, and has the potential to fabricate a large area of FTFH.

Table 1: Performance parameters of the printing material.

Performance	Nano-silver paste
Viscosity	≥20 000 mPa · s (25°C)
Silver content	≥80%
Density	2.9 g/cm^3
Adhesion	4B (PET substrate, sintered at 60°C for 60 min)

3.2 Photoelectric properties of large area FTFH

Optical transmittance and sheet resistance are two most important technical indicators for evaluating the photoelectric performance of FTFH. For the FTFH with Ag-grid, the line width and pitch of the Ag-grid are the two main factors affecting optical transmittance and sheet resistance. In order to study the influences of line width and pitch on optical transmittance and sheet resistance, Ag-grids with an area of 80 mm × 80 mm and different line widths and pitches were fabricated on the PET substrate using the EFD micro-scale 3D printing. For each process parameter, three samples were prepared for study. After conductive treatment of Ag-grids, the measured results of the optical transmittance and sheet resistance are shown in Figure 4.

Figure 4 shows the effect and rule of line width and pitch on optical transmittance and sheet resistance (without considering the optical transmittance of PET). Figure 4A shows the effect of different line widths on the optical transmittance while keeping a 2 mm period of Ag-grid. Figure 4B shows the effect of different line widths on the sheet resistance while keeping a 2 mm pitch of Ag-grid. Figure 4C shows the effect of different pitches on the optical transmittance while keeping a 30 μm line width of Ag-grid. As shown in Figure 4A, the optical transmittance of Ag-grid increases with the decrease of line width while keeping a 2 mm pitch of Ag-grid. For example, the optical transmittance of Ag-grid decreases from 96% to 91.5% as the line width increases from 13 μm to 55 μm. It means that the optical performance of Ag-grid becomes worse to some extent. At the same time, as shown in Figure 4B, the sheet

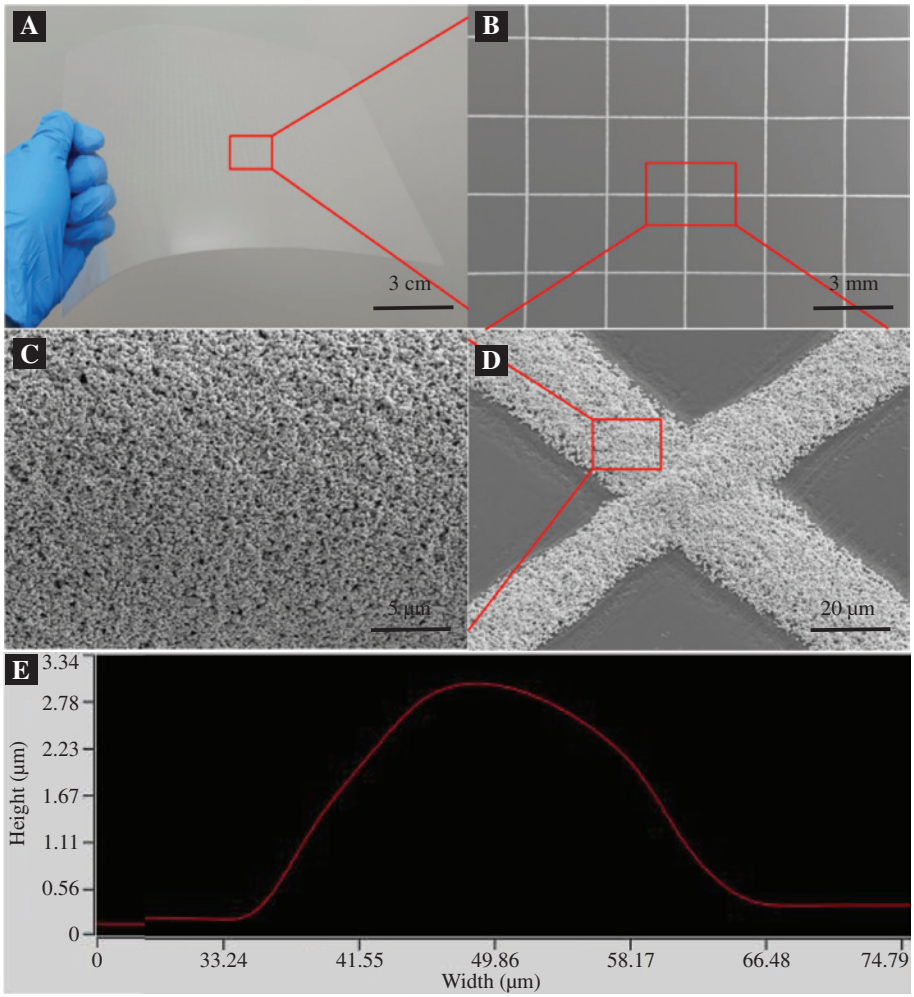

Figure 3: The macroscopic and microscopic morphology of the FTFH. (A) The macroscopic image of a FTFH; (B, C and D) magnification SEM images of Ag-grids; (E) section information of single Ag-line.

resistance of Ag-grid decreases with the increase of line width, and the decreasing trend becomes slower. Obviously, as the line width increases from 13 μm to 55 μm, the sheet resistance of Ag-grid decreases from 173 Ω sq^{-1} to 4.7 Ω sq^{-1}, which shows that the electrical performance of Ag-grid can be greatly improved by increasing the line width of Ag-grid.

As shown in Figure 4D, the optical transmittance increases gradually, and the sheet resistance increases linearly with the increase of the pitch of Ag-grid while keeping a 30 μm line width of Ag-grid. To summarise, the optical transmittance increases from 91.5% to 97.5% and the sheet resistance increases from 16.2 Ω sq^{-1} to 125 Ω sq^{-1} as the pitch increases from 1 mm to 6 mm. The results show that the high optical transmittance and low sheet resistance of the Ag-grid FTFH are contradictory. The FTFH with high optical transmittance requires a fine line width or a large pitch of the Ag-grid, while the sheet resistance of the Ag-grid is large at the same time. On the contrary, the low sheet resistance requires a wide line width or a small pitch of the Ag-grid, while the optical transmittance of the Ag-grid is low at the same time. By optimizing line width and pitch on the transmission and sheet resistance of Ag-grid, the FTFH can meet the requirements of different applications.

3.3 Electrothermal performances of large area FTFH

In order to further investigate the electrothermal performance of the FTFH, the FTFH with area of 80 mm × 60 mm, pitch of 2 mm and line width of 55 μm was used for the heating test. Figure 5A is the schematic diagram for the heating test of Ag-grid FTFH. Figure 5B shows the temperature responses under different voltages which was measured by an infrared camera. A DC power supply was

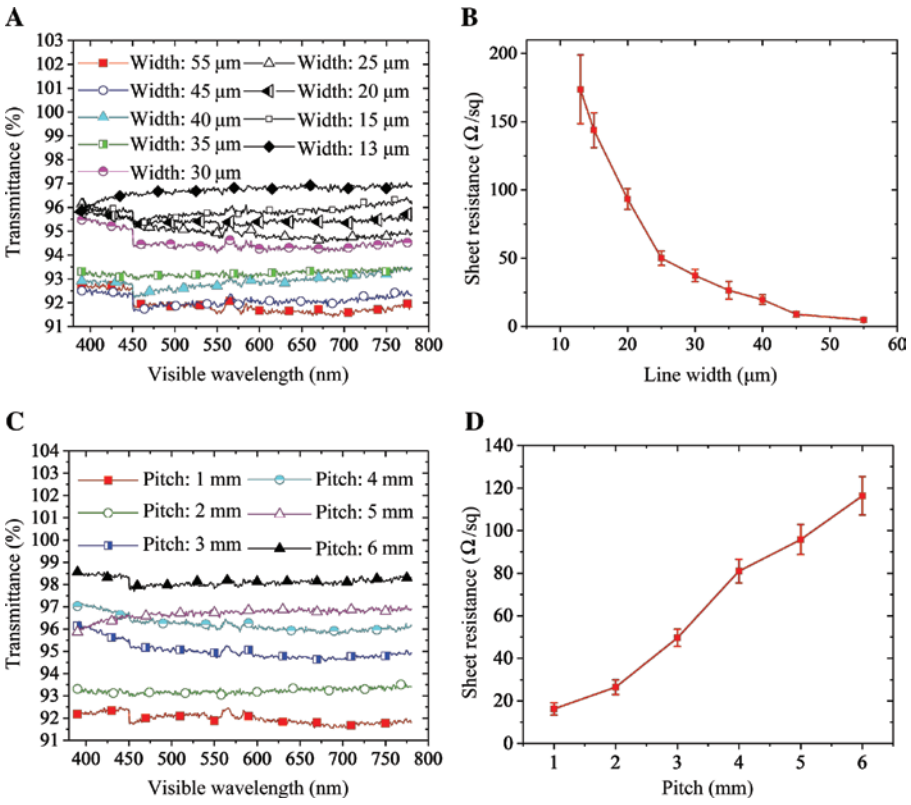

Figure 4: The effect and rule of line width and pitch on optical transmittance and sheet resistance. (A) Effect of line width on optical transmittance; (B) effect of line width on sheet resistance; (C) effect of pitch on optical transmittance; (D) effect of pitch on sheet resistance.

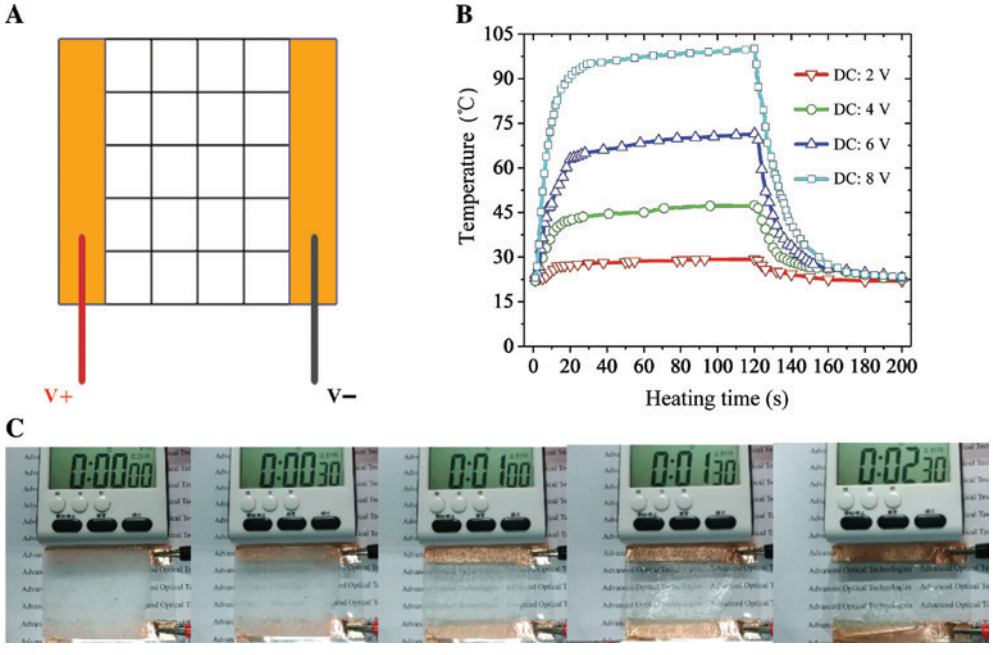

Figure 5: Heating test (A) principle of electrification; (B) heating time and temperature; (C) melting snow test.

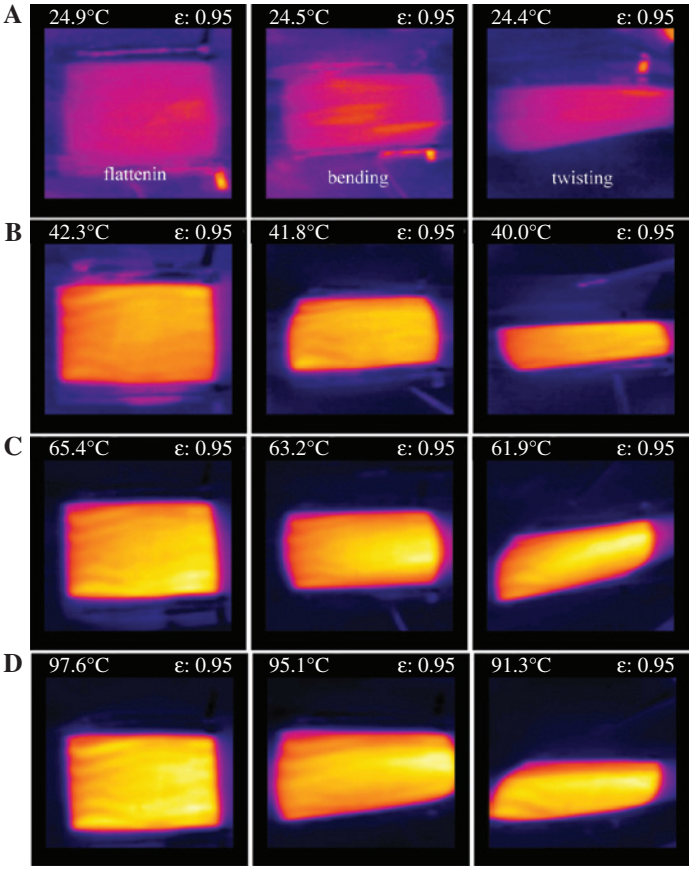

Figure 6: Testing of flexible heating (A) heating for 30 s at 2 V voltage; (B) heating for 30 s at 4 V voltage; (C) heating for 30 s at 6 V voltage; (D) heating for 30 s at 8 V voltage.

applied to provide input voltage. According to Figure 5B, the temperature response of FTFH can be divided into three stages: the heating stage (0–30 s), the equilibrium stage (30–120 s) and the cooling stage (120–200 s). In the heating stage, the temperature rises rapidly over time. In the equilibrium stage, the temperature rises very slowly. In the cooling stage, the temperature of FTFH decreases rapidly with the increase of time after the power supply is disconnected (120–150 s). The temperature decreases slowly after 150 s, and drops to room temperature until 200 s. In addition, the equilibrium temperature increases from 29.3 to 100.1°C as the input DC voltage increases from 2 to 8 V. Figure 5C shows the deicing effect of the FTFH at 6 V voltage. A snow block with a thickness of 5 mm was placed on the back of the Ag-grid. As shown in Figure 5C, the field of vision is very blurred before the power is turned on. After turning on the power for a short time, the snow block in the heating area on the back of FTFH starts melting, and the field of vision becomes clear gradually. After 150 s, almost all of the snow block covered on the heating area is melted.

In addition, we carried out a simple flexible heating test for FTFH. In Figure 6, are the infrared heating images of FTFH in different states such as, flattening, bending and twisting, which are electrified for 30 s with 2 V (Figure 6A), 4 V (Figure 6B), 6 V (Figure 6C) and 8 V (Figure 6D) voltage. The results show that the heating temperature of FTFH is similar to that of flat placement when it is bent and twisted, which indicates that the electrical conductivity (sheet resistance) of the FTFH has little change when it is bent and twisted. These results suggested that the FTFH has good flexible electric heating function.

4 Conclusions

In conclusion, we have developed a novel method for fabricating large-area FTFH based on the EFD microscale 3D printing. The high viscosity, high silver content (80 wt.%) and nano-silver paste sintered at low temperature (60°C) was used as the printing material, and FTFH was fabricated by printing the Ag-grid on the PET

substrate. Compared with the existing methods for fabricating FTFH, the method proposed in this paper has the advantages of high-efficiency, high material utilization rate and large area manufacturing. It is straightforward to fabricate Ag-grid on the surface of PET with the material utilization rate of 100%, and it takes only 6 min to fabricate a FTFH with an area of 200 mm × 200 mm (the line width of 25 μm, and the pitch of 3 mm). Meanwhile, the method proposed in this paper has a strong printing capability, which can improve the electrical conductivity of Ag-grid by using ultra-high viscosity (20 000 mPa · s) and high silver content nano-silver paste. Furthermore, the method proposed in this paper is low-cost, highly efficient, and template-free in the whole process. It can flexibly design the line width and pitch of Ag-grid according to the requirements of photoelectric performance, and realize the manufacturing of individualized and small batch FTFH. Although the proposed method in this work can provide a novel industrial solution for mass production of large-area FTFH, there are still some challenges. As it is well known, the key indicators of FTFH are optical transmittance and sheet resistance, which are often contradictory. By improving the resolution and aspect ratio of silver wire, the conductivity of Ag-grid can be improved on the premises of ensuring the optical transmittance. The EFD micro-scale 3D printing technology used in this paper is suitable for printing large aspect ratio microstructures. Consequently, our future research work is to 3D print large aspect ratio and high resolution silver conductors, so as to further improve the optical and electrical properties of FTFH.

Acknowledgments: This project was supported by National Natural Science Foundation of China (Funder Id: http://dx.doi.org/10.13039/501100001809, Grant No. 51775288, 51705271) and the Key research and development plan of Shandong Province (Grant No. 2018GGX103022).

References

[1] Y. H. Yoon, J. W. Song, D. Kim, J. Kim, J. K. Park, et al. Adv. Mat. 19, 4284–4287 (2007).
[2] R. Gupta, K. D. M. Rao, S. Kiruthika, G. U. Kulkarni, ACS Appl. Mater. Int. 8, 12559–12575 (2016).
[3] T. Sannicolo, M. Lagrange, A. Cabos, C. Celle, J. P. Simonato, et al. Small 12, 6052–6075 (2016).
[4] J. J. Bae, S. C. Lim, G. H. Han, Y. W. Jo, D. L. Doung, et al. Adv. Func. Mater. 22, 4819–4826 (2012).
[5] H. Kim, H. Lee, I. Ha, J. Jung, P. Won, et al. Adv. Func. Mater. 28, 1801847 (2018).
[6] T. Yamada, Y. Hayamizu, Y. Yamamoto, Y. Yomogida, A. Izadi-Najafabadi, et al. Nat. Nanotech. 6, 296–301 (2011).
[7] S. Hong, H. Lee, J. Lee, J. Kwon, S. Han, et al. Adv. Mater. 27, 4744–4751 (2015).
[8] S. Soltanian, R. Rahmanian, B. Gholamkhass, N. M. Kiasari, F. Ko, et al. Advan. Ener. Mater. 3, 1332–1337 (2013).
[9] Z. Wu, Z. Chen, X. Du, J. M. Logan, J. Sippel, et al. Science. 305, 1273–1276 (2004).
[10] M. Zhang, S. Fang, A. A. Zakhidov, S. B. Lee, A. E. Aliev, et al. Science 309, 1215–1219 (2005).
[11] D. S. Hecht, L. Hu, G. Irvin, Adv. Mater. 23, 1482–1513 (2011).
[12] L. R. Shobin, S. Manivannan, Sol. Ener. Mater. Sol. Cells 174, 469–477 (2018).
[13] K. S. Kim, Y. Zhao, H. Jang, S. Y. Lee, J. M. Kim, et al. Nature 457, 706–710 (2009).
[14] X. Li, G. Zhang, X. Bai, X. Sun, X. Wang, et al. Nat. Nanotech. 3, 538–542 (2008).
[15] H. Sun, D. Chen, C. Ye, X. Li, D. Dai, et al. Appl. Sur. Sci. 435, 809–814 (2018).
[16] M. Vosgueritchian, D. J. Lipomi, Z. Bao, Adv. Func. Mater. 22, 421–428 (2012).
[17] M. N. Gueye, A. Carella, R. Demadrille, J.-P. Simonato, ACS App. Mater. Inter. 9, 27250–27256 (2017).
[18] C. Celle, C. Mayousse, E. Moreau, H. Basti, A. Carella, et al. Nano Res. 5, 427–433 (2012).
[19] S. An, H. S. Jo, D. Y. Kim, H. J. Lee, B. K. Ju, et al. Adv. Mater. 28, 7149–7154 (2016).
[20] C. H. Lee, Y. J. Yun, H. Cho, K. S. Lee, M. Park, et al. J. Mater. Chem. C 6, 7847–7854 (2018).
[21] J. Schneider, P. Rohner, D. Thureja, M. Schmid, P. Galliker, et al. Adv. Func. Mater. 26, 833–840 (2016).
[22] D. Lordan, M. Burke, M. Manning, A. Martin, A. Amann, et al. ACS Appl. Mater. Inter. 9, 4932–4940 (2017).
[23] P. Lu, F. Cheng, Y. Ou, M. Lin, L. Su, et al. Comp. Sci. Tech. 153, 1–6 (2017).
[24] J. Kang, Y. Jang, Y. Kim, S. Cho, J. Suhr, et al. Nanoscale 7, 6567–6573 (2015).
[25] S. Ye, A. R. Rathmell, Z. Chen, I. E. Stewart, B. J. Wiley, Adv. Mater. 26, 6670–6687 (2014).
[26] J. A. Spechler, T. W. Koh, J. T. Herb, B. P. Rand, C. B. Arnold, et al. Advan. Funct. Mater. 25, 7428–7434 (2015).
[27] C. F. Guo, T. Sun, Q. Liu, Z. Suo, Z. Ren, et al. Nat. Commun. 5, 3121 (2014).
[28] T. Iwahashi, R. Yang, N. Okabe, J. Sakurai, J. Lin, et al. Appl. Phys. Let. 105, 223901 (2014).
[29] I. Burgués-Ceballos, N. Kehagias, C. M. Sotomayor-Torres, M. Campoy-Quiles, P. D. Lacharmoise, Sol. Energy Mater. Sol. Cells 127, 50–57 (2014).
[30] R. Eckstein, G. Hernandez-Sosa, U. Lemmer, N. Mechau, Org. Elect. 15, 2135–2140 (2014).
[31] Y. Jang, J. Kim, D. Byun, J. Phys. D: Appl. Phys. 46, 155103 (2013).